Entropy generation analysis of electrodialysis

Karim M. Chehayeb, John H. Lienhard V*

Department of Mechanical Engineering, Massachusetts Institute of Technology, Cambridge, MA 02139, USA.

Abstract

Electrodialysis (ED) is a desalination technology with many applications. In order to better understand how the energetic performance of this technology can be improved, the various losses in the system should be quantified and characterized. This can be done by looking at the entropy generation in ED systems. In this paper, we implement an ED model based on the Maxwell-Stefan transport model, which is the closest model to fundamental equations. We study the sources of entropy generation at different salinities, and locate areas where possible improvements need to be made under different operating conditions. In addition, we study the effect of the channel height, membrane thickness, and cell-pair voltage on the specific rate of entropy generation. We express the second-law efficiency of ED as the product of current and voltage utilization rates, and study its variation with current density. Further, we define the useful voltage that is used beneficially for separation. We derive the rate of entropy generation that is due to the passage of ions through a voltage drop, and we investigate whether voltage drops themselves can provide a good estimate of entropy generation.

Keywords: least work, efficiency, energy, thermodynamics, salinity

K.M. Chehayeb and J.H. Lienhard V, "Entropy generation analysis of electrodialysis," *Desalination*, online 24 March 2017, **413**:184-198, 1 July 2017.

*Corresponding author
Email address: lienhard@mit.edu (John H. Lienhard V)

Nomenclature

Acronyms

AEM	anion-exchange membrane
CEM	cation-exchange membrane
MS	Maxwell-Stefan

Symbols

A	area [m^2]
a	activity [-]
c	concentration [mol/m^3]
D	diffusion coefficient of salt [m^2/s]
$Đ_{ij}$	Maxwell-Stefan diffusion coefficient for species i and j [m^2/s]
F	Faraday constant, 96,487 [C/mol]
f	friction factor [-]
h	channel height [m]
i	current density [A/m^2]
i_{lim}	limiting current density [A/m^2]
J	flux [mol/m^2-s]
K_{ij}	friction coefficient for interaction of species i and j, $J.s/m^5$
L_{s}	salt permeability [m/s]
M	molar mass [g/mol]
m	molality [mol/kg]
N	number of moles [mol]
P	absolute pressure [Pa]
Q	volumetric flow rate [m^3/s]
R	universal gas constant, 8.314 [J/mol-K]
Re	Reynolds number [-]
r_{CP}	total cell-pair resistance [Ωm^2]
S	salinity [g/kg]
S	entropy [J/K]
$\dot{S}_{\text{gen}}$	entropy generation rate [W/K]
$\dot{s}'''_{\text{gen}}$	volumetric rate of entropy generation [W/m^3-K]
$\dot{s}''_{\text{gen}}$	entropy generation rate per unit area [W/m^2-K]
Sc	Schmidt number [-]
Sh	Sherwood number [-]
T	absolute temperature [K]
t	time [s]
t_{s}	effective transport number [-]
U	internal energy [J]
V	voltage [V]
v	velocity [m/s]
$\dot{W}$	work input [W]
x	spacial coordinate [m]

z	charge number

Greek

Δ	difference or change
∇	gradient
ε	spacer volume fraction [-]
Φ	electric potential [V]
$\gamma_{\pm}$	mean molal activity coefficient [-]
μ	dynamic viscosity [Pa s]
μ_i	electrochemical potential of ion i [J/mol]
μ_{s}	chemical potential of the salt [J/mol]
μ_{w}	chemical potential of water [J/mol]
μ^{θ}	chemical potential at the reference state [J/mol]
ξ_i	current utilization rate [-]
ξ_V	voltage utilization rate [-]
ρ	density [kg/m^3]

Subscripts

C	concentrate
co	co-ion
cou	counter-ion
CP	cell-pair
D	diluate
i	ion i
m	membrane / at membrane interface
s	salt
w	water

Superscripts

m	in membrane
s	in solution

1. Introduction

Electrodialysis (ED) is a desalination technology that takes in a work input in the form of an electric current that flows between two electrodes. These two electrodes are separated by fluid channels, which are bounded by cation-exchange and anion-exchange membranes placed in alternating order, as shown in Fig. 1. A cation-exchange membrane (CEM) preferentially lets cations through, and an anion-exchange membrane (AEM) preferentially lets anions through. This configuration, along with the applied voltage, results in the stream flowing in half of the channels becoming more dilute and the stream in the other half becoming more concentrated. The diluate and concentrate streams leave the ED stack in alternating order.

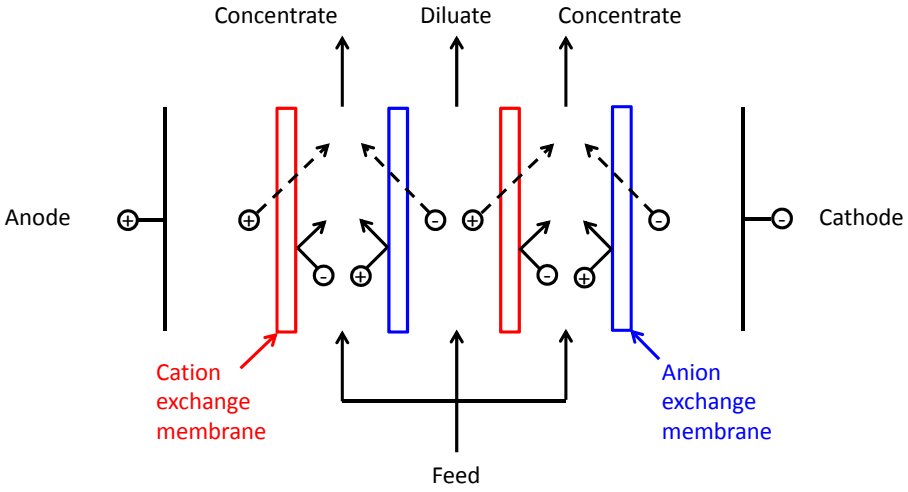

Fig. 1: Schematic diagram representing the operating principle of electrodialysis.

ED has many applications in the food and beverage industry. Some of the products manufactured using ED include dairy goods, wine, fruit juice, and sugar [1]. ED is widely used for the desalination of brackish water [2, 3], and has been shown to be suitable for the concentration of high-salinity feeds in the production of salt [3, 4].

Although ED has been in the market for decades, few studies have examined the thermodynamics of ED systems. McGovern et al. [5] defined thermodynamic metrics for efficiency and productivity, and they studied the local cost of desalination for different applications. Koter [6] studied the effect of channel height, diffusion layer thickness, membrane transport number, diluate salinity, and current density on the current efficiency and energy efficiency of the ED system.

Evaluating the thermodynamics of ED system, especially the causes of irreversibility (or entropy generation), is essential to improving the energy efficiency of these systems. Entropy generation analysis can be thought of as a diagnosis of the system. It locates and quantifies the losses in the system under different operating conditions. This identifies the major sources of losses that should be tackled in order to improve

the energy efficiency of the system. This analysis also determines which part of the electrical work input is used beneficially (i.e., for the purpose of separation) and which part is simply dissipated and why. Reducing the entropy generation in a system results in a direct reduction in its energy consumption as seen in the following equation, which is derived in detail in Appendix A:

$$\dot{W} = \dot{W}_{\text{least}} + T\dot{S}_{\text{gen}} \tag{1}$$

where $\dot{W}$ is the work input into the system, $\dot{W}_{\text{least}}$ is the least work of separation, T is the temperature of the system, and $\dot{S}_{\text{gen}}$ is the rate of entropy generation.

In this paper, we study the sources of entropy generation in an ED system, and we look at how the magnitudes of these losses vary at different operating conditions. This analysis guides the improvement of the technology at different salinities. In addition, we look at possible improvements to the system by studying the effect of channel height and membrane thickness. We study the effect of the cell pair voltage on the entropy generation in the system. Also, we define a useful voltage (that which contributes to ion separation) and compare voltage drops to entropy generation in order to determine whether voltage drops can be used to estimate the system losses.

2. Existing electrodialysis models

Several approaches to modeling electrodialysis can be found in the literature. Lee et al. [7] and Tsiakis and Papageorgiou [8] make several assumptions that are only valid for brackish water desalination, and model a complete electrodialysis desalination plant without examining the details of ion transport. The simplifying assumptions used in these papers are not valid when modeling the desalination of high-salinity feeds.

Fidaleo and Moresi [9] use a model based on the Nernst-Planck equations. This approach inherently assumes an ideal solution, which is not valid at high salinity. In addition, the model neglects kinetic coupling between the different components in the solution. The authors, however, manage to model the operation of ED up to a salinity of around 90 g/kg. They accomplish this by defining a water transport number that estimates the kinetic coupling between water and salt, and they empirically fit several membrane parameters in the range of the desired operation.

McGovern et al. [10] use the same approach and manage to model a multi-stage ED system operating in batch mode. The membrane parameters are empirically fitted at different salinities so that the model can predict the performance in a wide salinity range, reaching 192 g/kg.

Ortiz et al. [11] use a similar approach to model a single-stage batch ED system used in treating brackish water. The main idea behind these models [9–11] is that the flux of salt through the membranes can be

divided into two parts: migration, which is proportional to the applied current density, and diffusion, which is proportional to the concentration difference across the membrane. Similarly, the water flux is assumed to be a result of migration, where water is dragged by the moving ions, and osmosis, which is proportional to the difference in osmotic pressure across the membrane.

Tedesco et al. [12, 13] extend the Nernst-Planck equation to the membrane, and model the water transport through the membrane using the Maxwell-Stefan equation.

Kraaijeveld et al. [14] use a Maxwell-Stefan-based approach to model the use of ED in the desalination of a solution of NaCl-HCl, and Pintauro and Bennion [15] measure the Maxwell-Stefan (MS) diffusion coefficients of NaCl in a Nafion membrane. The MS model is the most accurate model for concentrated solutions in the presence of electrostatic forces [16, 17]. Unlike the Nernst-Planck model, the MS model does not assume the solution is ideal. In addition, the Maxwell-Stefan-based model captures electro-osmosis through the membrane naturally through kinetic coupling, whereas the Nernst-Planck-based model requires a separate fitting parameter in the form of a water transport number to capture that effect. In addition, the MS equation is the more general expression, and simplifies to the Nernst-Planck equation if we neglect kinetic coupling by limiting the forces felt by each species to those exerted by the solvent, and if, in addition, we assume that the solution is ideal.

From a different perspective, the MS equation writes the expression for flux in a fashion consistent with the theory of irreversible thermodynamics. The phenomenological coefficients in irreversible thermodynamics and the MS diffusion coefficients can in fact be theoretically related to one another [17–19]. It has been shown, however, that the MS coefficients are less dependent on composition (total dissolved solids, as well as the different ions present) than are the phenomenological coefficients [20].

According to Fidaleo and Moresi [9], the Nernst-Planck-based model is more appropriate to model the performance of a specific system given that the fitting parameters are easier to measure. However, given that the goal of the present paper is the thermodynamic analysis of ED, we will use the MS model because it is closer to fundamental equations and better captures the true driving forces. That said, the results presented in this paper have been qualitatively replicated by the present authors using the Nernst-Planck-based model, and are not specific to the MS model.

3. Modeling

As explained in the previous section, the model that is the closest to the fundamentals, and that is valid at high salinities, is that based on the MS equations as reported by Kraaijeveld et al. [14]. In this section, we present the major components of the model that will be used in the proposed research. In this paper,

the change in salinity along an ED stack is not modeled, and the focus is on the local level, which can be modeled at a single location with one pair of salinities.

3.1. Hydrodynamics

An ideal ED model would accurately model the fluid dynamics inside the channels. In other words, the ideal model would solve the Navier-Stokes equations coupled with the salt transport equations and Poisson's equation. However, this set of equations is very complex and requires a numerical solution, which would limit the scope of the simulation to a small section of the channel without any regard to what is happening at the level of the complete system; this also makes it very difficult to model the fluxes with the appropriate boundary conditions across the membranes. The major effect of fluid flow on the performance of ED is that it enhances the mass transfer by making the boundary layer thinner. This effect can be captured by using the stagnant film theory as is commonly used in modeling ED [9–11, 14]. This model assumes that the fluid inside the channel is very well mixed, except for a thin boundary layer of thickness δ that is adjacent to each membrane, where

$$\delta = \frac{2h}{\mathrm{Sh}} \tag{2}$$

and the Sherwood number, Sh, is the dimensionless number representing the mass transfer coefficient. Previous attempts of empirically measuring the Sherwood number can be found in the literature [21, 22]. In this paper, we will use the correlation developed by Kuroda et al [23]:

$$\mathrm{Sh} = 0.25\ \mathrm{Re}^{\frac{1}{2}}\mathrm{Sc}^{\frac{1}{3}} \tag{3}$$

Figure 2 shows the boundary later thickness, δ, and the channel height, h.

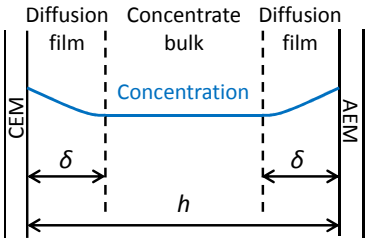

Fig. 2: Schematic diagram showing the boundary layer thickness, δ, and the channel height, h.

3.2. Transport inside the diffusion film

Each Maxwell-Stefan equation can be thought of as a force balance, where the driving force on a species is equal to the friction forces exerted on this species by the other species present inside the solution:

$$-\frac{c_i}{RT}\nabla\mu_i = \frac{1}{RT}\sum_{j=1}^{n} K_{ij}\left(v_i - v_j\right) = \sum_{j=1}^{n}\frac{c_i c_j}{c_{tot}\text{Đ}_{ij}}\left(v_i - v_j\right) \tag{4}$$

where Đ_{ij} are the MS diffusion coefficients, defined according to the above equation. K_{ij} is a friction factor, v_i is the velocity of species i, averaged over all the particles of the same species, and μ_i is the electrochemical potential of species i:

$$\mu_i = RT\ln a_i + z_i F\Phi + \mu_i^{\theta} \tag{5}$$

where a_i is the activity of species i, Φ is the electric potential, and μ_i^{θ} is the chemical potential at the reference state. We can replace the velocity by the mole flux of the species, $J_i = c_i v_i$, and rearrange the MS equation:

$$-c_i\nabla\ln a_i - \frac{z_i c_i F}{RT}\nabla\Phi = \sum_{j=1}^{n}\frac{c_j J_i - c_i J_j}{c_{tot}\text{Đ}_{ij}} \tag{6}$$

For a system of n species, we have $n-1$ independent MS equations, as the MS equation of the n^{th} species can be obtained from the first $n-1$ MS equations using the Gibbs-Duhem equation, and is therefore not independent.

In describing the electric potential profile, the more fundamental equation linking the electric potential to the charges of the ions is Poisson's equation. In the regions where the Laplacian of the electric potential, $\nabla^2\Phi$, is not great, this equation reduces to the electroneutrality equation:

$$\sum_i z_i c_i = 0 \tag{7}$$

The only region where this condition fails is in the electric double layer, which occurs at the interface between the solution and the membrane and has a thickness between 1 and 10 nm [17]. However, we can consider the electric double layer as part of the interface and treat it separately from the solution where we can use the electroneutrality equation. A thorough discussion on the validity of the electroneutrality equation is given by Newman and Thomas-Alyea [17].

3.3. Transport through the membranes

At the membrane-solution interface, we assume that each species that is present in the two media is at thermodynamic equilibrium. In addition, we use the activity coefficients of the species inside the membranes

as measured by Kraaijeveld et al. [14] to determine the concentrations of the ions at the membrane surface. The equations describing this equilibrium are presented in Appendix B.

The MS equations are also used to model the salt and water transport through the membranes. One difference between the equations used inside the membrane and those used in the diffusion film is that the fixed charge of the membrane is added as a new species. In addition, the diffusion coefficients are different inside the membrane. Also, the membrane velocity (or flux) is set to 0 because the membrane is stationary [14]. Given that we do not have the activities of the different species inside the membrane away from the surface, we can apply the MS equations by treating the membrane as one finite element and taking the differences between the two sides of the membrane where the properties are known. In addition, we can use average values of the concentrations at the two surfaces of the membrane to approximate the concentration at the center of the membrane. At steady state, the fluxes of salt and water through the membrane are equal to those in the adjacent diffusion layers. We assume that heat is dissipated fast enough to keep the systems studied at a constant temperature, T.

3.4. Electric potential profile

The voltage of the cell pair is equal to the sum of all the voltage drops in the cell pair

$$V_{\mathrm{CP}} = \left(r_{\mathrm{bulk,C}} + r_{\mathrm{bulk,D}}\right) i + \Delta\Phi_{\mathrm{CEM}} + \Delta\Phi_{\mathrm{AEM}} + \Sigma_{j=1}^{4}\Delta\Phi_{\mathrm{film,j}} \tag{8}$$

where i is the current density, and $r_{\mathrm{bulk,C}}$ and $r_{\mathrm{bulk,D}}$ are the bulk resistances in the concentrate and diluate channels, respectively, and are calculated from experimental data on conductivity [24–26]. The electric potential drops in the membranes, $\Delta\Phi_{\mathrm{CEM}}$ and $\Delta\Phi_{\mathrm{AEM}}$, and in each of the four films, $\Delta\Phi_{\mathrm{film,j}}$, are calculated using the MS equations described above. We note that the Donnan potential drops are included in the membrane potential drops given that we treat the interface a part of the membrane.

The solution procedure used to solve the equations in the model is presented in Appendix B. The system characteristics used in the modeling are presented in Appendix C, and a discussion on the use of sodium chloride as the electrolyte is presented in Appendix D. Finally, the numerical model is validated against experimental results from the literature in Appendix E.

4. Calculating entropy generation

The volumetric rate of entropy generation from transport can be written as

$$\dot{s}'''_{\mathrm{gen}} = \sum_{k} \nabla F_k \cdot \boldsymbol{J}_k \tag{9}$$

Table 1: The driving forces for different extensive properties, where F_k is defined by Eq. 11.

Extensive property, X_k	**Driving force, ∇F_k**
Internal energy, U	$\nabla\left(\frac{1}{T}\right)$
Volume, V	$\nabla\left(\frac{P}{T}\right)$
Number of moles of species j, N_j	$\nabla\left(\frac{-\mu_j}{T}\right)$

where $\boldsymbol{J}_k$ is the flux of the extensive property, X_k:

$$\boldsymbol{J}_k \equiv \frac{1}{A}\frac{dX_k}{dt} \tag{10}$$

where A is area, and t is time. ∇F_k is the driving force associated with X_k (also called affinity, conjugate force, or generalized force), and F_k is defined as

$$F_k = \frac{\partial S}{\partial X_k} \tag{11}$$

where S is the total entropy. The driving forces for different extensive properties are shown in Table 1. These equations can be derived from first principles as shown by Callen [27] and Bejan [28].

The volumetric rate of entropy generation due to diffusion then is

$$\dot{s}'''_{\text{gen}} = \sum_k \nabla\left(\frac{-\mu_k}{T}\right) \cdot \boldsymbol{J}_k \tag{12}$$

and the volumetric rate of entropy generation due to fluid flow is

$$\dot{s}'''_{\text{gen}} = -\frac{\boldsymbol{Q}}{A} \cdot \nabla\frac{P}{T} \tag{13}$$

The expression for the total entropy generation rate of the entire channel was expressed by Bejan [29] as:

$$\dot{S}_{\text{gen}} = \frac{Q\Delta P}{T} \tag{14}$$

where Q is the volumetric flow rate, ΔP is a positive pressure drop, and T is the temperature. The calculation of the pressure drop is shown in Appendix F.

5. Sources of entropy generation in electrodialysis

In this section, we study the different sources of entropy generation in ED and we look at how the contribution of each source varies with the salinities of the concentrate and diluate channels. Total entropy generation is divided by location: CEM and AEM membranes, concentrate and diluate channels, and the diffusion films between each membrane and the bulk of the channel. In order to be able to compare the operation of ED under different salinities, we fixed the value of the electric current to 75 A/m^2, which was below the limiting current at the lowest concentration studied. The current was fixed instead of the voltage because losses in an electric system are mostly rate dependent, and, therefore, a fixed current would result in a better comparison.

Given that salinity varies along the length of an ED stack, the effect of a salinity pair can only be isolated by studying the entropy generation rate locally. At given concentrate and diluate salinities, channel height, and membrane characteristics, the entropy generation rate can be calculated locally on a per unit area basis without the need to specify the length of the system or update the salinities using a mass balance.

5.1. Effect of salinity on the spatial distribution of entropy generation

In an ED cell pair, the concentrate and the diluate have different salinities at most locations. To simplify the presentation of results, only three concentrate-to-diluate salinity ratios are presented: 1, 2, and 3. At a salinity ratio of 1, both salinities are set to the same value and are varied from 2 g/kg to 150 g/kg. The division of the entropy generation between the different sources is presented in Fig. 3. At low salinities, most of the entropy is generated in the fluid channels as a result of the high electric resistivity of low-salinity solutions. This phenomenon is well understood in ED, and possible solutions, such as the use of conductive spacers [30, 31], have been proposed. At higher salinities, the resistivity of the solutions decreases and the membranes become the dominant sources of entropy generation. In fact, the entropy generation rate inside the membranes is a weak function of salinity, and salinity affects the distribution of entropy generation by changing the resistivity of the solutions.

We can conclude from this graph that the design of channels and spacers is very important at low salinity but not as important at high salinity. For example, at 100 g/kg, around 80% of the losses occur in the membranes which means that targeting the channels can at most decrease the losses by 20%. In reality, the improvement will be much less than the full reversible (lossless) limit, which means that any significant improvement of the energetic performance of a high-salinity system has to be directed at the membranes. Similarly, any significant improvement at low salinity has to be directed at the fluid channels. The dashed line at 21 g/kg indicates the salinity at which the major source of entropy generation switches from the

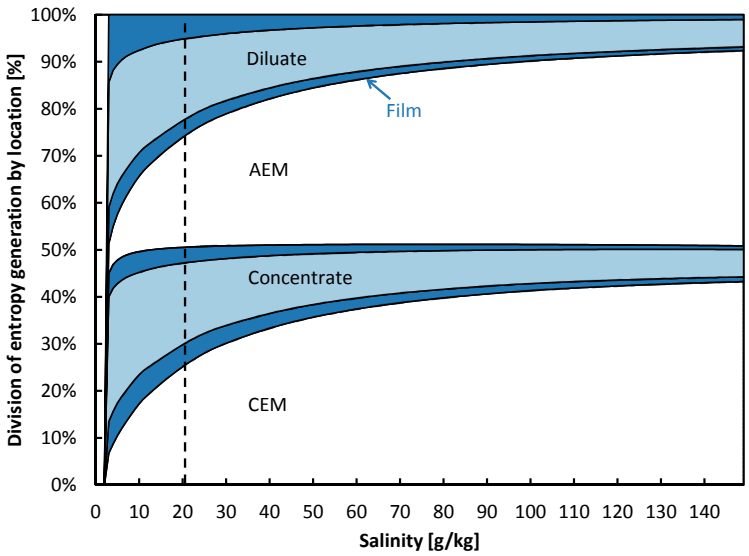

Fig. 3: The division of the entropy generation by source at different salinities. $h = 1$ mm in both channels, and Sh $= 18$. $S_{\mathrm{C}} = S_{\mathrm{D}}$.

channels to the membranes. This specific salinity is only valid for this particular system, but can provide a general estimate to what is meant by low salinity and high salinity.

Figure 4 shows the division of the entropy generation by source for: a) a concentrate-to-diluate salinity ratio of 2; and b) a ratio of 3. As was the case for a salinity ratio of 1, the fluid channels are the dominant source of losses at low salinity, and the membranes dominate at high salinity. There two main differences between the results presented in Fig. 4 and those presented in Fig. 3. The first is that the diluate channel generates more entropy than the concentrate channel, which is expected given the difference in their concentrations. The second is that more entropy is generated in the membranes than for the case with equal concentrations. This is because the higher salinity difference results in more osmosis and diffusion. This last point can be seen by comparing the fraction of entropy that is generated in the diluate channel for a ratio of 2 and a ratio of 3. It can be seen that, at the same diluate salinity, the diluate channel constitutes a bigger portion of the total entropy generation at the lower salinity ratio, and the membranes generate more entropy for the higher concentrate-to-diluate salinity ratio.

5.2. Viscous losses in electrodialysis

The previous section was limited to study of entropy generation due to transport in the direction through the membranes. If the goal is to improve the energetic performance of the entire system by tackling only these sources, entropy generation due to lateral transport has to be the dominant fraction of the total entropy generation. Figure 5 shows that, at current densities used in most practical applications, most of the entropy generation is indeed due to transport, and not to viscous effects. The fraction of losses due to viscous effects

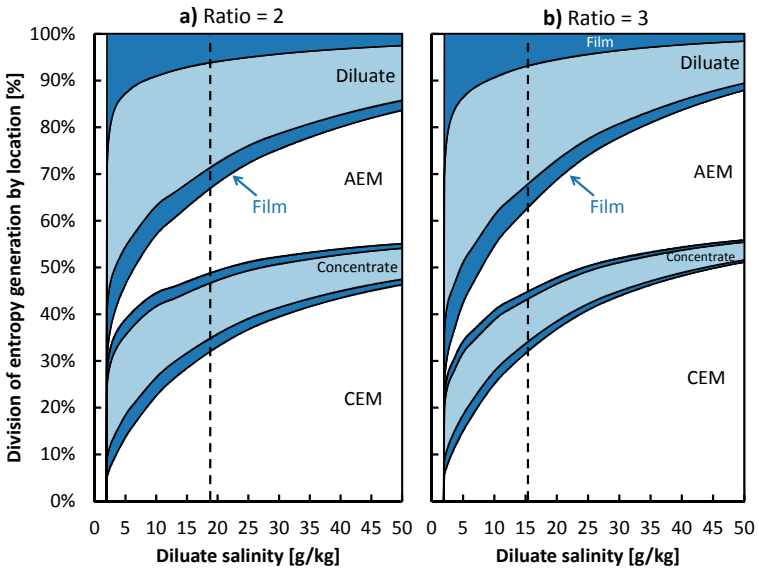

Fig. 4: The division of the entropy generation by source at different salinities. $h = 1$ mm in both channels, and Sh $= 18$. a) $S_{\mathrm{C}} = 2S_{\mathrm{D}}$, and b) $S_{\mathrm{C}} = 3S_{\mathrm{D}}$.

becomes very small at high currents, which means that significant energetic improvements can be made by focusing on reducing the losses due to transport. For these results, the velocity was set to 10 cm/s, and the channel height was set to 1 mm, which are typical values for ED systems. In addition, entrance effects were neglected to enable a location-independent study of viscous losses. This is an acceptable approximation given that the correlations used are for channels with spacers, and that a typical ED stack length is much larger than the channel height. Further, looking at the rate of entropy generation per unit area enables the calculation of local viscous losses without the need to integrate over a stack length. We note here that these

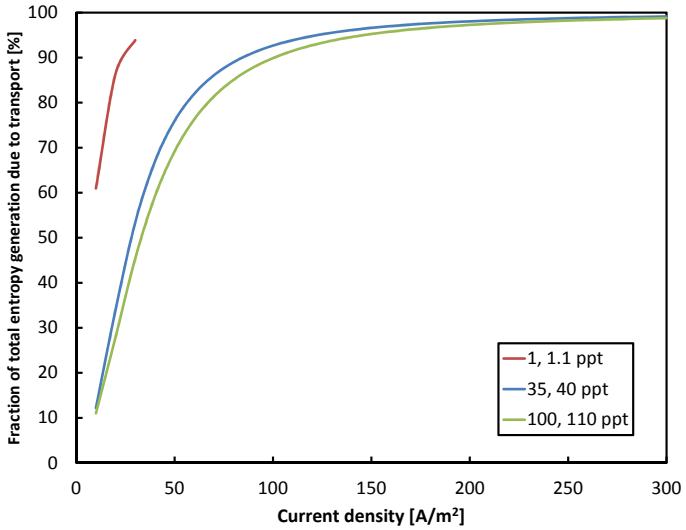

Fig. 5: The fraction of the total entropy generation that is due to transport at different current densities. This fraction can be referred to as a modified Bejan number [32].

results show the entropy generation due to viscous effects inside the stack. In reality, more losses also occur inside the pump, manifolding, and the piping. An inefficient pump would obviously increase the importance of hydraulic losses.

The choice of velocity affects the viscous losses much more than it affects the transport losses. The chosen velocity of 10 cm/s in Fig. 5 is on the higher end of typical ED velocities, and the conclusion that transport losses dominate is not affected by going to slightly higher velocities. Decreasing the channel height decreases the transport losses and increases the viscous losses, thereby decreasing the fraction of the total entropy generation that is due to transport. Given that high-salinity systems are operated at high current densities, the only situation in Fig. 5 for which viscous losses are significant is at low salinity. However, at low salinities, the decrease in channel height results in an increase in the limiting current density, and higher current densities counter viscous losses. This is how brackish water ED systems are operated.

5.3. Effect of channel height

In an ED cell pair treating low-salinity water, most of the losses occur in the fluid channel. The area resistance of the fluid channel is the product of the resistivity of the solution and the channel height. Given that the concentration of the fluid in the channel is set by the application, we can only vary the channel height to reduce the resistance. Figure 6 shows the effect of the channel height on the entropy generation normalized per mole of salt removed. The system simulated has a concentrate salinity, S_{C}, equal to 2 g/kg and a diluate salinity, S_{D} equal to 1 g/kg. The volumetric flow rate of the system is kept constant to keep the capital costs of the different systems constant (i.e., the same membrane area per unit feed), which means that the product of bulk velocity and channel height is kept constant. The velocity is set to the typical value of 10 cm/s at the typical channel height of 1 mm. The total entropy generated is divided into entropy generated through mass transport (in the direction through the membrane) and entropy generated through viscous losses (fluid flow along the membrane). The entropy generation due to transport increases linearly with increasing channel height, due to the increased channel resistance, and the entropy generation due to viscous effects decreases quadratically with increasing channel height, as can be shown from the equations in Appendix F. The two opposing effects result in the total specific entropy generation having a clear minimum. The numbers presented in this graph are dependent on the system modeled, but this result frames the design of the optimal channel height as a balance between electric resistance and pumping power. At low salinity, the balance is delicate, as seen in Fig. 6. At high salinity, given the low resistivity of the channels, the viscous losses are important and a higher channel height is preferred. In real system design, the objective function will be the total power consumption, which is the sum of the power consumed by the ED stack to desalinate and the pumping power. Inefficient pumps and highly saline solutions push the optimal design to wider channels.

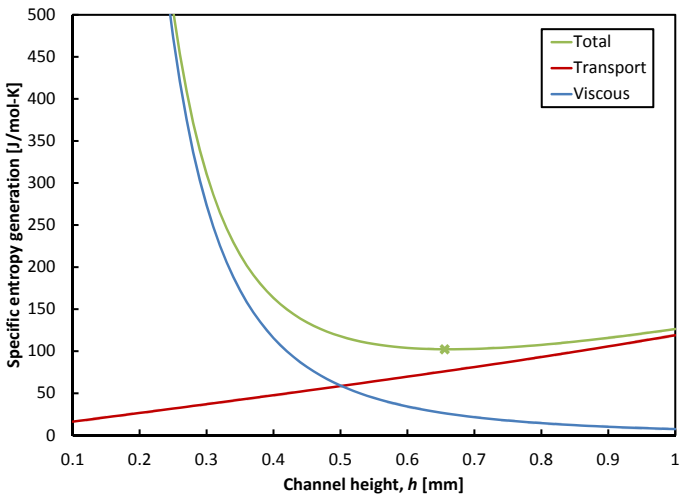

Fig. 6: The effect of channel height on the specific entropy generation. $S_{\mathrm{D}} = 1$ g/kg, $S_{\mathrm{C}} = 2$ g/kg, and $i = 35$ A/m^2

5.4. Effect of membrane thickness

At high salinity, most of the losses occur inside the membranes. Just like the channel height, we can think of the membrane electric resistance as being proportional to the membrane thickness. Figure 7 shows the variation of specific entropy generation with the membrane thickness for two systems: one with a small difference in salinity and the other with a large difference. For the system at low salinity difference, decreasing the membrane thickness decreases the total entropy generated in the system. This is not the case at the high salinity difference, where decreasing the membrane thickness results in a significant increase in entropy generation. The high salinity difference results in high driving forces for osmosis and diffusion across the membranes. This is shown in Fig. 8, where membrane thickness does not have a strong effect on the salt and water fluxes for the system at the low salinity difference. As for the system with the higher salinity difference, decreasing the membrane thickness from 1 mm to 0.35 mm increases the water flux by around 50% and greatly decreases the salt flux.

The conclusion from this result is that a thinner membrane thickness is beneficial only if the salinity difference is kept low or if the water permeability is greatly decreased. Although a thin membrane reduces the electric resistance, it also reduces the resistance to mass transport through diffusion and osmosis. These effects only become significant when the driving forces are high enough. At low salinity difference, energetic considerations motivate a thinner membrane, and the optimal membrane thickness is then determined by how thin the membrane can be while still remaining robust and tolerating cleaning.

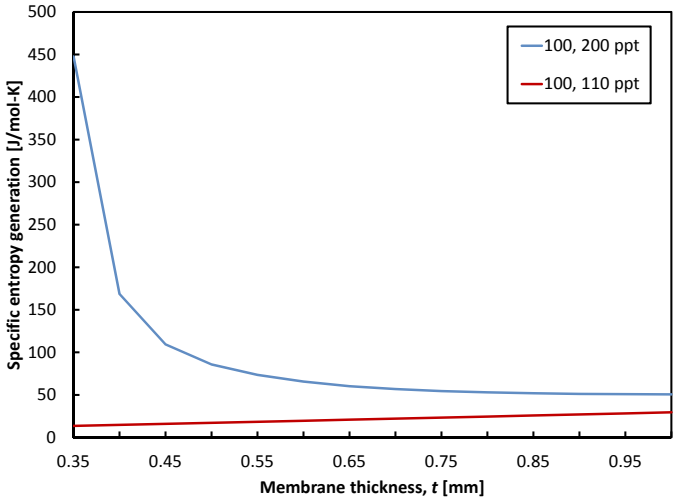

Fig. 7: The effect of membrane thickness on the specific entropy generation. $i = 75$ A/m^2

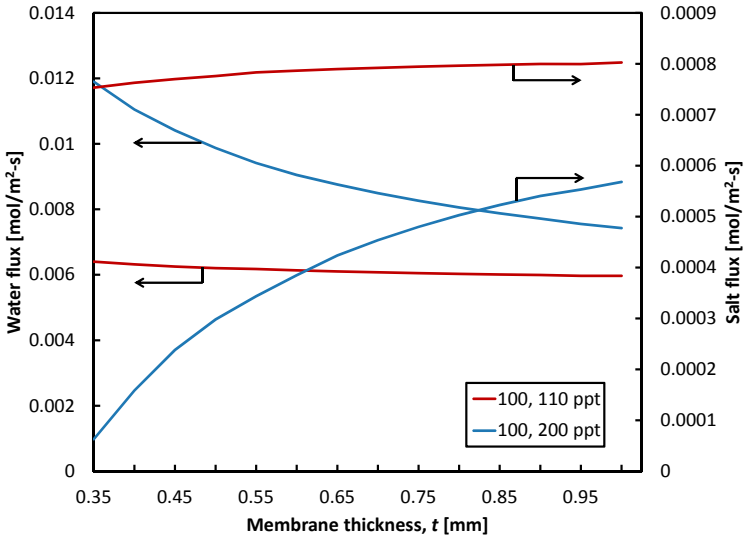

Fig. 8: The effect of membrane thickness on salt and water fluxes through the membrane. $i = 75$ A/m^2

6. Minimizing entropy generation in ED

In this section, we study the effect of the cell pair voltage on the entropy generation in the ED system. The required energy input is minimized when the entropy generation in the system is minimized, and more of the work input goes into achieving the goal of ED, which is the transfer of salt from the diluate channel to the concentrate channel.

6.1. Can the process be reversible?

Figure 9 shows that the total entropy generation rate due to transport is minimized when the two ionic fluxes through the membrane are equal, or, in other words, when there is no electric current. Even though the minimum total flux (in absolute value) occurs at around 0.055 V, entropy is still generated in the two

channels because of the passage of current. An interesting trend that is apparent from this figure is that the applied voltage can never result in both ionic fluxes being 0. The applied voltage can set the flux of the counter-ion to 0 because it acts in the direction opposite to the chemical potential driving force, such that the net driving force for the counter-ion can be set to 0. The applied voltage, however, cannot set the flux of the co-ion to 0. In the CEM modeled here, diffusion will cause the co-ion to flow in the negative direction, and the applied voltage will also drive the co-ion in that direction. Similarly, the applied voltage can never block osmosis because the voltage actually results in an electro-osmotic water flow in the same direction as that of osmosis. Therefore, we can conclude that an ED stack with different concentrations in the diluate and concentrate channels cannot result in a reversible process at any applied voltage because there will always be fluxes of ions and water which cannot be stopped by the applied voltage. The only reversible systems would be either one with equal diluate and concentrate concentrations or one using perfectly perm-selective membranes (which do not allow the passage of co-ions) which also blocked the passage of water molecules, with the applied voltage in both systems set such that the flux of the counter-ion is infinitely small[1].

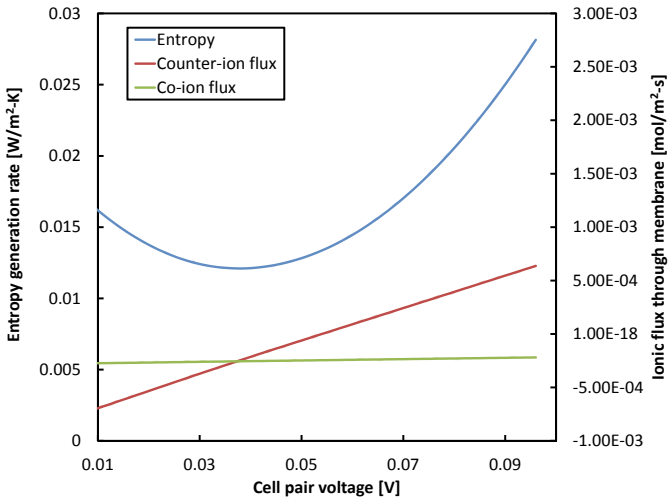

Fig. 9: The effect of cell pair voltage on the ionic fluxes and transport entropy generation in an ED cell pair. $S_D = 100$ g/kg and $S_C = 200$ g/kg.

6.2. How should the voltage be set?

Figure 10 shows the variation of specific entropy generation with cell pair voltage. Focusing first on the entropy generation due to diffusion and migration, we see that it is minimized at a voltage close to that which results in no electric current flow. The results reported in the figure start at the lowest voltage which results

[1]The applied voltage that results in no current flow is that equal and opposite to that faced by the membrane due to being subject to different activities. For a single membrane, this voltage can be supplied by reversible electrodes placed in the solutions adjacent to the membrane. The potential difference between the two electrodes is only due to the difference in the activities of the solutions and will be equal and opposite to that of the membrane, resulting in no net potential drop.

in a positive salt flux, and the reason for the apparent singularity at low cell-pair voltage is that the initial salt flux is very small. This initial decrease of specific entropy generation due to diffusion and migration can also be explained by looking at the efficiency of the system, which will be done in Section 7. This figure shows that from an energetic perspective, the ED stack should be operated at the voltage that is just large enough to overcome the electric potential generated by having different concentrations in the two channels. An explicit expression for this voltage is derived in Section 7.

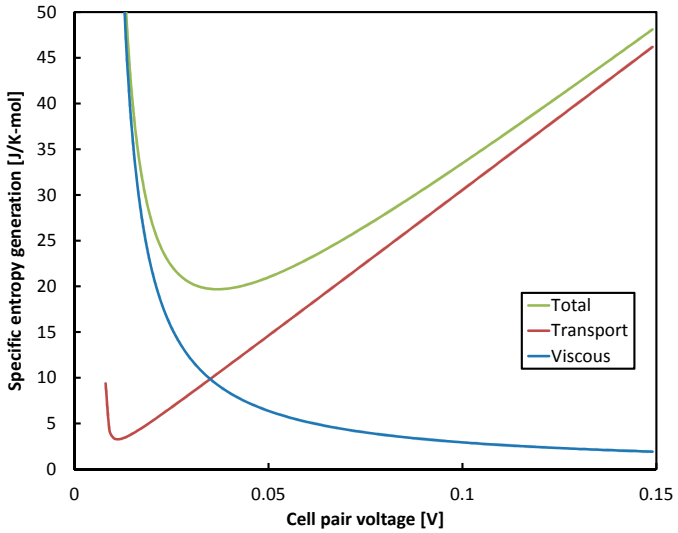

Fig. 10: The effect of of voltage of the specific entropy generation in an ED cell pair. $S_{\mathrm{D}} = 35$ g/kg and $S_{\mathrm{C}} = 40$ g/kg.

Figure 10 also shows the variation of the specific entropy generation due to viscous effects. The velocity and stack geometry are not varied, therefore the total viscous losses are constant. The decreasing specific rate of viscous entropy generation is due to the increasing salt flux with increasing voltage. This shows that even though the energy input to the stack is minimized when the current is zero, the pumping power still needs to be considered. The figure shows an optimal operating voltage specific to this case, but the competing effects of voltage on transport losses and viscous losses are general: for each case, there exists a cell pair voltage that minimizes the total specific rate of entropy generation.

In addition, we should consider the required membrane area. The modeling in this work focuses on local entropy generation. A real ED system, however, needs to remove a specific amount of salt. At small current density (and salt fluxes), large membrane surfaces are required to remove a specific amount of salt. The specific ED-stack power input is minimized at close to the lowest possible voltage, while the capital costs are minimized at the highest possible voltage: the optimal operating voltage has to be determined through an economic analysis, which factors in the price of electricity, the price of membranes, and other capital costs.

7. Second-law efficiency

As shown in detail in Appendix A, the least work to take $J_s\,dA$ of salt from a concentrate of salinity S_C to a diluate salinity of S_D can be written as:

$$\dot{W}_{least} = J_s \Delta\mu_s\,dA \tag{15}$$

where J_s is the salt flux and $\Delta\mu_s$ is the difference in salt chemical potential between the concentrate and diluate channels and is positive. The salt flux can be written as a function of the current density by defining the current utilization rate, ξ_i, which, for a binary salt, is defined as

$$\xi_i = \frac{FJ_s}{i} \tag{16}$$

which can at best be equal to 1.

We can then define a second-law efficiency as:

$$\eta = \frac{\dot{W}_{least}}{\dot{W}_{electric}} = \frac{\xi_i \Delta\mu_s}{FV_{CP}} \tag{17}$$

where the actual work input is:

$$\dot{W}_{electric} = iV_{CP}\,dA = \frac{FJ_s}{\xi_i} V_{CP}\,dA \tag{18}$$

From Eq. 17 we can also back out a 'useful voltage', which represents the voltage actually used for separation rather than for overcoming losses:

$$V_{useful} = \frac{\Delta\mu_s}{F} = 2\frac{RT}{F} \ln \frac{\gamma_{\pm,C} m_C}{\gamma_{\pm,D} m_D} \tag{19}$$

where $\gamma_\pm$ is the mean molal activity coefficient, and m is the molality. This expression, like the Nernst equation for electrodes, simply relates the required electric potential drop to the salt activities in the two channels. The same expression can also be reached by setting the entropy generation in the membranes to be zero. For each membrane, the driving force for the counter-ion is set to zero, which allows us to write the required membrane potential drop as a function of the activities of the counter-ion in the two channels. Summing the two membrane potential drops results in the expression for useful voltage reached above.

From Eq. 17, we can then define a voltage utilization rate, ξ_V, which is the ratio of the useful voltage to the applied voltage:

$$\xi_V = \frac{V_{useful}}{V_{CP}} = \frac{\Delta\mu_s}{FV_{CP}} \tag{20}$$

The expression for efficiency can then be written as the product of the current and voltage utilization rates:

$$\eta = \xi_i \xi_V \tag{21}$$

Figure 11 shows the effect of the current density on the efficiency and on the current and voltage utilization rates. The current utilization rate increases with increasing current density. This can be explained by looking at the expression for salt flux as described by Fidaleo and Moresi [9]:

$$J_s = \frac{t_s i}{F} - L_s \Delta c \tag{22}$$

where t_s is the cell-pair salt transport number, with $t_s \leq 1$, and L_s is the permeability, which is a proportionality constant for diffusion from the concentrate to the diluate. Both factors are independent of the current density. The current utilization rate can be expressed as:

$$\xi_i = t_s - \frac{F L_s \Delta c}{i} \tag{23}$$

The current utilization rate starts with negative values at very low current density, and converges to t_s as i becomes large enough. When the concentration difference between the two channels is small, the salt flux is directly proportional to the current density, and the voltage that results in no salt flux also results in no current flow.

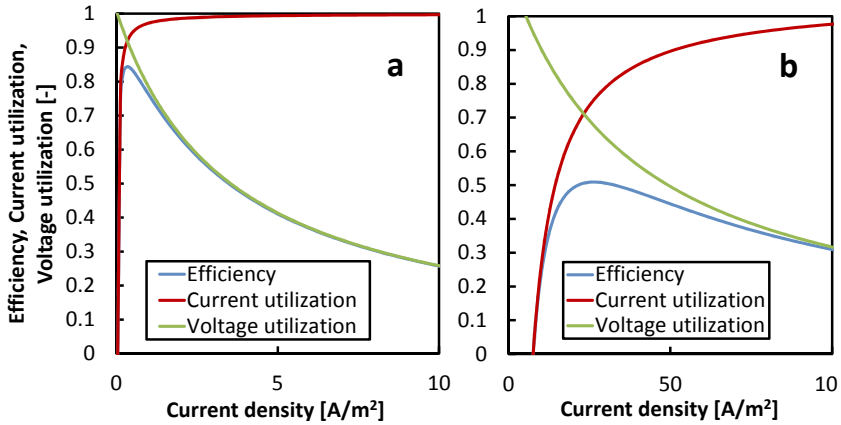

Fig. 11: The effect of current density on efficiency, current utilization rate, and voltage utilization rate at: a) $S_D = 1$ g/kg and $S_C = 2$ g/kg; and b) $S_D = 35$ g/kg and $S_C = 70$ g/kg.

Using the MS equations, it can be shown that the voltage losses in the channels (including the diffusion films) and in the membranes (other than the useful voltage) are purely ohmic losses due to friction between the different ions, the solvent, and the membranes. The diffusion film also adds to the resistance by reducing the

concentration and conductivity in the diluate channel such that the additional resistance becomes significant when the system is operating near the limiting current density.

Another type of voltage loss is the additional voltage that has to be spent above the useful voltage due to concentration polarization. Concentration polarization results in a higher concentrate concentration next to the membrane, $c_{\mathrm{C,m}}$, and a lower diluate concentration on the other side of the membrane, $c_{\mathrm{D,m}}$. As a result, the minimum voltage that has to be applied to overcome this concentration difference, at zero current, is then similar to the expression in Eq. 19, with the updated activities to reflect the concentrations just outside the membranes. Figure 12 shows that there are no potential drops in the channels and films when there is no current flow, and the useful voltage is the only potential drop.

The cell-pair voltage can then be written as the sum of the useful voltage, the ohmic losses, and the contribution of concentration polarization described above:

$$V_{\mathrm{CP}} = V_{\mathrm{useful}} + r_{\mathrm{CP}} i + 2\frac{RT}{F} \ln \frac{c_{\mathrm{C,m}} c_{\mathrm{D}}}{c_{\mathrm{D,m}} c_{\mathrm{C}}} \tag{24}$$

where it is assumed that the activity coefficients do not vary greatly with the concentration changes due to concentration polarization. Equation 24 explains the variation of the voltage utilization rate with current density. As shown in Fig. 11, the voltage utilization rate starts at a value of 1 when there is no net salt flux, and decreases as the current density increases. In addition, the voltage utilization rate decreases faster in the first case, where the concentrate and diluate salinities are lower and the cell-pair resistance is higher.

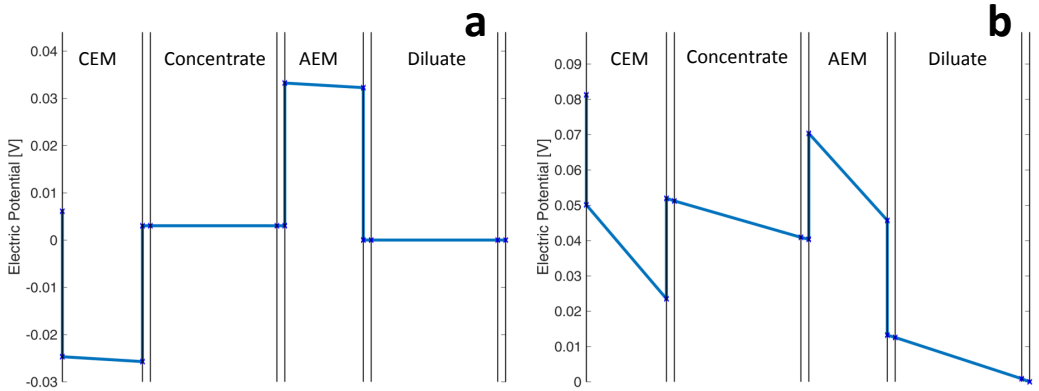

Fig. 12: The electric potential profile for a diluate at 35 g/kg and a concentrate at 40 g/kg at: a) 0 A/m^2; and b) 75 A/m^2.

As shown in the first case presented in Fig. 11, when the concentration difference between the concentrate and diluate channels is small, the current utilization rate increases rapidly and reaches a high value even at low current density. A system with a small concentration difference can, therefore, achieve a high efficiency when it is operated at low current density that is high enough to result in a high current utilization rate. By comparing the two cases shown in Fig. 11, it is clear that the higher concentration difference requires going

to higher current densities to achieve high current utilization rates. However, going to high current densities decreases the voltage utilization rate, and, as a result, systems with a large salinity difference cannot achieve high efficiency values regardless of the operating current density.

The expression for efficiency defined in Eq. 17 includes losses due to non-perfect current and voltage utilization rates. A third type of loss that does not feature in Eq. 17 is that due to water transport, which reduces the volume of the diluate and dilutes the concentrate. When the goal is to desalinate, the required amount of diluate and its salinity are set. In this case, a system with significant osmosis and electro-osmosis requires the desalination of a larger diluate stream, which translates into a larger work input to remove a larger amount of salt, and a combination of larger channels (more electrical losses) and a larger pumping requirement. When the goal is to concentrate a stream (for zero-discharge desalination or salt production), this type of loss requires the removal of larger amounts of salt, which translates into higher energy requirements.

McGovern et al. [5] included the effect of water flux in their definition of efficiency. In deriving our definition of efficiency, we set salt removal as the goal of the energy input, whereas McGovern et al. [5] set the change in free energy as the goal of the process. The effect of the water flux on the efficiency is similar to that of diffusion: both are stronger when the concentration difference is larger, and both are independent of current, and so their effect decreases with increasing current density.

Finally, we can relate efficiency to the rate of entropy generation:

$$\eta = \frac{\dot{W}_{\text{least}}}{\dot{W}_{\text{electric}}} = \frac{\dot{W}_{\text{least}}}{\dot{W}_{\text{least}} + T\dot{S}_{\text{gen, transport}}} \tag{25}$$

where $\dot{S}_{\text{gen, transport}}$ is the rate of entropy generation due to the transport in the direction perpendicular to the membranes. In this expression, the viscous losses are not considered because we are looking at the efficiency of the local separation process. The efficiency is maximized when the rate of entropy generation due to transport is minimized. The effect of the current density on the efficiency, presented above, helps explain the initial decrease in the rate of specific entropy generation at low cell-pair voltage shown in Fig. 10. At low voltage (or current density), the low current utilization rate decreases the efficiency, and also increases the specific rate of entropy generation. Hence, the voltage that minimizes the specific rate of entropy generation due to transport is slightly larger than V_{useful}, with higher concentration differences requiring larger voltages.

8. Using voltage drops to estimate losses

In this section, we link voltage drops to the entropy generation rate, and look into whether voltage drops are a good approximation of losses. It has been shown in Section 4 that the volumetric entropy generation

rate can be calculated as follows

$$\dot{s}'''_{\text{gen}} = \sum_k \nabla \left(\frac{-\mu_k}{T} \right) \cdot \boldsymbol{J}_k \tag{9}$$

In the direction perpendicular to the membrane,

$$\dot{s}'''_{\text{gen}} = -\frac{1}{T} \left(J_+ \frac{d\mu_+}{dx} + J_- \frac{d\mu_-}{dx} + J_{\text{w}} \frac{d\mu_{\text{w}}}{dx} \right) \tag{26}$$

In the simple case where the concentrations do not vary with space, for example at a central location in the channels outside the diffusion layer, we can write:

$$\dot{s}'''_{\text{gen}} = -\frac{F}{T} \left(J_+ - J_- \right) \frac{d\Phi}{dx} = -\frac{i}{T} \frac{d\Phi}{dx} \tag{27}$$

Integrating along x, we get the entropy generation rate per unit area:

$$\dot{s}''_{\text{gen}} = -\frac{i \Delta\Phi}{T} \tag{28}$$

In the absence of concentration gradients, diffusion and osmosis are also absent, and fluxes are only driven by electro-migration and electro-osmosis. In these cases, all of the entropy generation is due to the current flowing across an electric potential drop, as shown above. However, when osmosis and diffusion occur due to chemical potential differences, more or less entropy is generated than that accounted for by only considering the electric driving force. In the cases where the concentration gradient contributes positively to the driving force (i.e., the gradient in the concentration increases the salt flux), the actual entropy generation rate will be higher than that calculated using only the current. One such example is the diffusion layer, which enhances the salt flux. The opposite happens inside the membranes, where the applied electric potential must overcome the chemical potential gradient. In that case, the concentration gradient drives the salt from the concentrate to the diluate, whereas the applied electric field drives the salt in the direction that desalinates the diluate. The resulting entropy generation rate is then smaller than that predicted by just considering that generated by the flow of current through a voltage drop.

Given that, for a specific location along the ED stack, the current density is the same in the membranes, channels, and diffusion films, Eq. 28 can be used to convert a voltage drop to a rate of entropy generation. In the following analysis, we look at whether voltage drops can be used to estimate the total local rate of entropy generation. As described above, Eq. 28 captures the full rate of entropy generation only in the bulk of the channels where there are no concentration gradients. Figure 13 shows that using the total voltage drop in Eq. 28 does not result in a good approximation of the actual entropy generation rate in the films and

membranes. This is consistent with the fact that not the entire voltage drop is necessarily a loss, such as in the membrane, and not every loss is necessarily captured by the voltage drop, such as in the diffusion films. In fact, the voltage drop across a membrane consists of a useful voltage drop and a voltage loss due to the resistance of the membrane:

$$V_{\text{loss}} = V - V_{\text{useful}} \tag{29}$$

In the presence of concentration gradients, going from Eq. 26 to Eq. 27 involves neglecting the following terms:

$$-\frac{1}{T}\left(J_{\text{cou}}RT\frac{d\ln a_{\text{cou}}}{dx} + J_{\text{co}}RT\frac{d\ln a_{\text{co}}}{dx} + J_{\text{w}}\frac{d\mu_{\text{w}}}{dx}\right) \tag{30}$$

where the subscripts 'cou' and 'co' refer to the counter-ion and the co-ion, respectively. As shown in Fig. 13, neglecting all of these terms results in a poor estimate of the actual rate of entropy generation. By neglecting the losses due to water transport (the third term in Eq. 30), and by assuming perfectly perm-selective membranes, we can rewrite Eq. 26 as:

$$\dot{s}'''_{\text{gen}} \approx -\frac{J_{\text{cou}}}{T}\frac{d\mu_{\text{cou}}}{dx} \tag{31}$$

and Eq. 28 as

$$\dot{s}''_{\text{gen}} \approx -\frac{iV_{\text{mod}}}{T} \tag{32}$$

where

$$V_{\text{mod}} = \frac{\Delta\mu_{\text{cou}}}{z_{\text{cou}}F} = \Delta\Phi_{\text{total}} + \frac{RT}{z_{\text{cou}}F}\Delta\ln a_{\text{cou}} \tag{33}$$

Equation 33 can be thought of as a generalized expression for Eq. 29, where the term 'loss' is dropped in favor of the term 'modified' so that the same definition can be extended to the diffusion layer, where the modified voltage, as defined in the equation above, is greater than the actual voltage drop because the concentration gradient adds to the driving force.

As shown in Fig. 13, using the modified voltage drop results in much better matching with the total entropy generation rate. However, when the concentration difference is large, osmosis and diffusion are no longer negligible, and, as a result, even the modified voltage is not always a good approximation of entropy generation. The expression only becomes acceptable at higher currents as the relative importance of osmosis and diffusion is reduced. Generally speaking, this condition is achieved when the current utilization rate, ξ_i, is close to 1. Using the modified voltage in general results in a good approximation of the losses in the system, but it does not capture the water flux and the effect of diffusion on the ionic fluxes. Ideally, the full expression of entropy generation should be used to guide the improvements of the system, but if a simpler expression is required, only the modified voltage expression should be used because the actual voltage will

result in poor estimates.

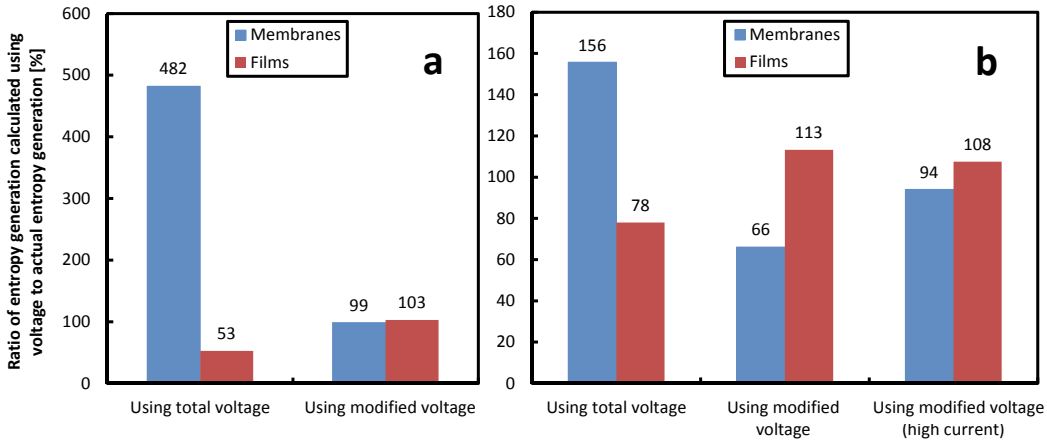

Fig. 13: The ratio of entropy generation calculated using voltage drops to actual entropy generation: a) at low salinity difference ($S_{\mathrm{D}} = 1$ g/kg and $S_{\mathrm{C}} = 1.1$ g/kg) with $\xi_i = 1.00$; and b) at high salinity difference ($S_{\mathrm{D}} = 35$ g/kg and $S_{\mathrm{C}} = 70$ g/kg) with $\xi_i = 0.90$ for the first and second columns, and $\xi_i = 0.99$ for the third column.

9. Conclusions

In this paper, we have looked at entropy generation in an ED system and studied its variation with salinity. The second-law efficiency was written as the product of current and voltage utilization rates. A useful voltage was defined, and the different sources of losses were characterized. We also linked voltage drops to entropy generation and investigated whether voltage drops can be used to approximate system losses.

The major conclusions from this work are the following:

1. At low salinity, most of the entropy is generated inside the fluid channels. In this case, efforts to decrease energy consumption should be focused on transport in the channels.
2. At high salinity, most of the entropy is generated inside the membranes. Decreasing the membrane electrical resistance is key to better performance at high salinity.
3. Thinner membranes can decrease entropy generation and energy consumption. However, thinner membranes also decrease the resistances to diffusion and osmosis, which means that the overall effect is beneficial only when the driving forces for these modes of transport are small, or when the membranes are very resistant to the passage of co-ions and water.
4. At high enough current density, most of the entropy is generated from salt and water transport, and not through viscous losses.
5. Given a specified volumetric flow rate, there exists an optimal channel height that minimizes the local entropy generation from transport and viscous effects.

6. Second-law efficiency is maximized, and specific entropy generation due to salt and water transport is minimized, at a voltage slightly larger than the useful voltage, with higher concentration differences requiring larger voltages. However, from a total energy efficiency perspective, the optimal voltage should minimize total entropy generation, including that from viscous losses.
7. A modified voltage which approximates the complete driving force to salt transport should be used in approximating entropy generation. These approximations are only valid at high enough current when osmosis and diffusion become relatively less important.

Acknowledgments

The authors would like to thank Kuwait Foundation for the Advancement Sciences (KFAS) for their financial support through Project No. P31475EC01.

Appendix A. Derivation of least work

We can derive the expression for the least work required to remove salt from a low concentration to a high concentration by studying the control volume shown in Fig. A.14. We assume that the amount of salt removed is small enough to not result in a change in the salinities of the streams: $J_\mathrm{s}\,dA \ll \dot{N}$. This condition is required to be able to calculate the least work required for two specific salinities: c_C and c_D.

We can write the first law of thermodynamics for the control volume shown in Fig. A.14:

$$J_\mathrm{s}\,dA\left(\bar{h}_\mathrm{C} - \bar{h}_\mathrm{D}\right) = \dot{W} + \dot{Q} \tag{A.1}$$

where $J_\mathrm{s}\,dA$ is the amount of salt removed, $\bar{h}$ is the molar specific enthalpy, $\dot{W}$ is the work input, and $\dot{Q}$ is the heat input from a source temperature, T, equal to that of the system.

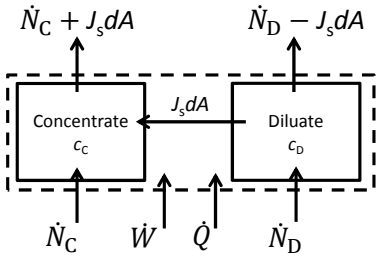

Fig. A.14: Schematic diagram of the control volume used for calculating the least work required to transport $J_\mathrm{s}\,dA$ of salt from a stream of concentration of c_D to a stream of concentration of c_C.

We can also write the second law of thermodynamics:

$$J_\mathrm{s}\,dA\left(\bar{s}_\mathrm{C} - \bar{s}_\mathrm{D}\right) = \frac{\dot{Q}}{T} + \dot{S}_\mathrm{gen} \tag{A.2}$$

where $\bar{s}$ is the molar specific entropy, and $\dot{S}_{\text{gen}}$ is the rate of entropy generation.

We can multiply the second equation by the temperature, T, and subtract it from the first equation, and get an expression for the work input as a function of the chemical potential difference, $\Delta\mu_{\text{s}}$, and the rate of entropy generation:

$$\dot{W} = J_{\text{s}}\, dA \left[\left(\bar{h}_{\text{C}} - T\bar{s}_{\text{C}}\right) - \left(\bar{h}_{\text{D}} - T\bar{s}_{\text{D}}\right)\right] + T\dot{S}_{\text{gen}} = J_{\text{s}}\, dA\, \Delta\mu_{\text{s}} + T\dot{S}_{\text{gen}} \tag{A.3}$$

The smallest work input is required when there is no entropy generation:

$$\dot{W}_{\text{least}} = J_{\text{s}} \Delta\mu_{\text{s}}\, dA \tag{15}$$

and

$$\dot{W} = \dot{W}_{\text{least}} + T\dot{S}_{\text{gen}} \tag{1}$$

Appendix B. Numerical solution procedure

Given the applied voltage and the bulk concentrations in the diluate and concentrate channels, we can calculate the ionic and water fluxes. The first step is to guess 5 fluxes in the cell pair: $J_{+,\text{CEM}}$, $J_{-,\text{CEM}}$, $J_{w,\text{CEM}}$, $J_{+,\text{AEM}}$, and $J_{w,\text{AEM}}$. The sixth flux, $J_{-,\text{AEM}}$, can be calculated through conservation of charge:

$$i = F\left(J_{+,\text{CEM}} - J_{-,\text{CEM}}\right) = F\left(J_{+,\text{AEM}} - J_{-,\text{AEM}}\right) \tag{B.1}$$

Given all the fluxes, we can use two independent MS equations inside each diffusion film to build the concentration and electric potential profiles. The two MS equations can be rearranged, and, using the fourth order Runge-Kutta method, the concentration profile can be calculated. The concentration profile and a second combination of the MS equations can then be used to build the electric potential profile.

At the interface, we assume that each species that exists in both media is in thermodynamic equilibrium:

$$\mu_i^m = \mu_i^s \tag{B.2}$$

$$RT \ln a_i^m + z_i F \phi^m = RT \ln a_i^s + z_i F \phi^s \tag{B.3}$$

The equilibrium equations for the cation and anion can be rearranged to give the following expression for the Donnan potential:

$$\Delta\phi_{\text{Donnan}} = \phi^m - \phi^s = \frac{RT}{z_i F} \ln \frac{a_i^s}{a_i^m} \tag{B.4}$$

Equating the resulting Donnan potential for the two ions results in the following equations:

$$\frac{a_+^s a_-^s}{a_+^m a_-^m} = 1 \tag{B.5}$$

$$\frac{c_+^s c_-^s}{c_+^m c_-^m} = \frac{\gamma_\pm^{m\,2}}{\gamma_\pm^{s\,2}} \tag{B.6}$$

where the activity coefficient inside the membrane, $\gamma_\pm^m$, can be determined experimentally [14]. We note that the activity coefficient is for the salt, and that there is no need for the activity coefficients of the separate ions as the equation above only uses the product of the activities. Equation B.6 is combined with the electroneutrality equation inside the membrane to calculate the concentrations of the two ions inside the membrane.

Given the concentrations at the interface, Eq. B.4 is used to calculate the Donnan potential. The expressions for the Donnan potential calculated using the anion and the cation are averaged:

$$\Delta\phi_{\text{Donnan}} = \frac{\Delta\phi_{\text{Donnan,+}} + \Delta\phi_{\text{Donnan,-}}}{2} \approx 0.5\frac{RT}{F}\ln\frac{c_-^m}{c_+^m} \tag{B.7}$$

This averaging helps in canceling out the activity coefficients of the separate ions by assuming that $\gamma_+ = \gamma_-$.

We can write three independent MS equations for each membrane because we have four species. As an example, we write the MS equation applied to water:

$$-c_{\text{w}}\nabla\ln a_{\text{w}} = \frac{c_+ J_{\text{w}} - c_{\text{w}} J_+}{c_{\text{tot}}\mathit{Đ}_{\text{w+}}} + \frac{c_- J_{\text{w}} - c_{\text{w}} J_-}{c_{\text{tot}}\mathit{Đ}_{\text{w-}}} + \frac{c_{\text{m}} J_{\text{w}}}{c_{\text{tot}}\mathit{Đ}_{\text{mw}}} \tag{B.8}$$

where the left-hand side is the driving force associated with the water flux, and the right-hand side is the sum of the friction forces acting on the water by the cation, the anion, and the membrane, respectively. The concentrations are taken as the average of those on either end of the membrane, but just inside the membrane. The gradient on the left-hand side is calculated as one difference between the two sides of the membrane divided by the thickness of the membrane, without further discretization of the membrane.

The three MS equations can be rearranged, and one of the resulting equations can be used to calculate the electric potential drop across the membrane, and the other two equations can be used as checks on the guessed fluxes. In addition, we can calculate the difference between the set voltage and the sum of all the voltage drops in the system, which should be set to 0. We have 2 MS equations in each membrane, and the cell-pair voltage equation, totaling 5 equations where all the quantities are known. We can write these 5 equations in the form

$$f(\mathbf{J}) = 0 \tag{B.9}$$

which is the function we need to solve by guessing the fluxes, **J**. The roots of the function, i.e. the correct fluxes, are then calculated iteratively using MATLAB's *fsolve* function.

Appendix C. System characteristics

Table C.2: The diffusion coefficients outside the membranes as reported by Kraaijeveld et al. [14]. Original data from Chapman [33] and Mills and Lobo [34]. c is the solution concentration in mol/m^3.

Components	**Diffusivity** [10^{-9} m^2/s]
Na^+, H_2O	1.333
Cl^-, H_2O	2.033
Na^+, Cl^-	0.0015 $c^{0.65}$

Table C.3: The diffusion coefficients inside the membranes (in 10^{-10} m^2/s), measured and calculated by Kraaijeveld et al. [14].

Components	**61 CZL 386**	**204 UZL 386**
Na^+, Cl^-	0.24	0.19
Na^+, H_2O	3.12	0.75
Na^+, Membrane	0.31	0.16
Cl^-, H_2O	1.81	5.12
Cl^-, Membrane	0.31	0.51
H_2O, Membrane	2.49	4.93

Table C.4: Membrane characteristics measured by Kraaijeveld et al. [14]. c is the solution concentration in mol/L.

Membrane property	**61 CZL 386**	**204 UZL 386**
Capacity [mol/m^3 wet membrane]	1690	1827
Thickness [mm]	0.563	0.551
Density of wet membrane, ρ_m [kg/m^3]	1167.5 - 7.5c + 7.5c^2	1100.0 + 15.0c
Salt activity coefficient, $\gamma_{\pm}^m$ [-]	0.57 + 0.28c	0.56 + 0.29c
Water content [%]	30.17 - 0.83c	33.38 - 1.42c

Water concentration inside the membrane is calculated from the water content and membrane density

$$c_w^m = \frac{\%H_2O \times \rho_m}{100 M_w} \tag{C.1}$$

Appendix D. Thermophysical properties

The complexity of the model used increases greatly with the presence of additional species. For this reason, it was decided to only model a binary salt. A solution of sodium chloride was chosen as the electrolyte because experimental data on the diffusion coefficients and activity coefficient of sodium chloride inside the membranes were found in the literature [14]. In addition, sodium chloride is the major component in seawater, and the most recent property correlations of seawater [35] show close agreement with those of sodium chloride [36]. Further, sodium chloride serves as an acceptable substitute in estimating the properties of certain high-salinity waters [37]. The properties of sodium chloride were taken from an implementation by Thiel et al. [37, 38] of Pitzer's equations [39–44]. The properties of that were used are the solution density, the activity coefficient, and the water activity.

Appendix E. Validation of the model

The modeling procedure used in this paper is based on the work done by Kraaijeveld et al. [14, 45], which also reports experimental results and measured diffusion coefficients. To validate our model with the reported experimental results, we also modeled a solution of HCl-NaCl. Given that the electrode equations used in that work were not very clear, we used the reported experimental values of the current density. Instead of setting the cell-pair voltage, we set the current density to the experimental value. Given the experimental current density, the model is used to determine the fluxes of the different ions and that of the water. This resulted in very good matching between our model and the reported concentrations, as shown in Fig. E.15. The variation of the concentrations with time is a direct result of all the fluxes, which means that the transport through the membranes is modeled accurately.

Ideally, we should also be able to validate the resistance network by comparing the total calculated voltage to that measured in the same experiments. However, given that this was not possible, this part of the modeling was verified by comparing the film resistances to those calculated using experimental values of resistivity. In addition, the membrane voltage difference is calculated from the MS equations used to determine the fluxes through the membranes. Given that the fluxes through the membranes are predicted accurately, as discussed above, we can safely assume that the calculated membrane voltage drop is also accurate, especially given that the 3 MS equations in each membrane need to be solved simultaneously to get the fluxes, and two of them need to be combined to result in the membrane voltage drop. For additional assurance, the calculated membrane resistances were compared to typical values reported in the literature and were found to be within the appropriate range.

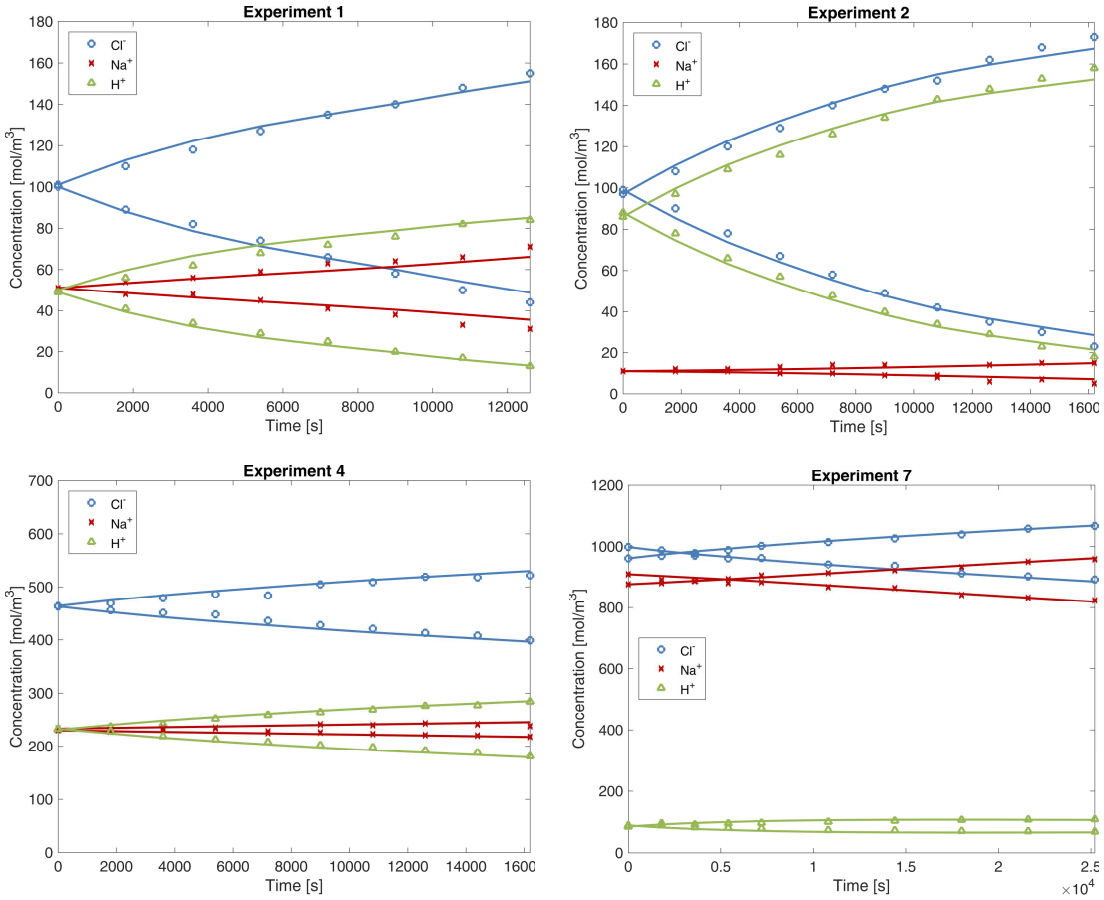

Fig. E.15: Validation of the model using experiments from the literature [45]. The symbols represent experimental values and the solid lines represent the modeling results.

Appendix F. Pressure drop calculation

We can write the pressure drop inside the ED channel as

$$\Delta P = 4f\frac{L}{D_\mathrm{e}}\frac{\rho v^2}{2} \tag{F.1}$$

The correlation by Kuroda et al. [23] is used to calculate the friction factor:

$$f = k_\mathrm{f}\mathrm{Re}^{-\frac{1}{2}} \tag{F.2}$$

where k_f is a spacer property also defined by Kuroda et al. D_e is the effective diameter defined as

$$D_\mathrm{e} = \frac{2hW\left(1-\epsilon_\mathrm{s}\right)}{h+W} \tag{F.3}$$

where h is the channel height and W is the channel width. Given that $W \gg h$

$$D_{\mathrm{e}} = 2h\,(1 - \epsilon_{\mathrm{s}}) \tag{F.4}$$

$$\mathrm{Re} = \frac{\rho v D_{\mathrm{e}}}{\mu\,(1 - \epsilon_{\mathrm{s}})} = \frac{2\rho v h}{\mu} \tag{F.5}$$

References

[1] M. Fidaleo, M. Moresi, Electrodialysis applications in the food industry, Advances in Food and Nutrition Research 51 (2006) 265–360. doi:10.1016/S1043-4526(06)51005-8.
URL http://dx.doi.org/10.1016/S1043-4526(06)51005-8

[2] N. C. Wright, A. G. Winter V, Justification for community-scale photovoltaic-powered electrodialysis desalination systems for inland rural villages in India, Desalination 352 (2014) 82–91. doi:10.1016/j.desal.2014.07.035.
URL http://dx.doi.org/10.1016/j.desal.2014.07.035

[3] H. Strathmann, Electrodialysis, a mature technology with a multitude of new applications, Desalination 264 (2010) 268–288. doi:10.1016/j.desal.2010.04.069.
URL http://dx.doi.org/10.1016/j.desal.2010.04.069

[4] T. Nishiwaki, Concentration of electrolytes prior to evaporation with an electromembrane process, Industrial Processing with Membranes. New York: John Wiley.

[5] R. K. McGovern, S. M. Zubair, J. H. Lienhard V, The cost effectiveness of electrodialysis for diverse salinity applications, Desalination 348 (2014) 57–65. doi:10.1016/j.desal.2014.06.010.
URL http://dx.doi.org/10.1016/j.desal.2014.06.010

[6] S. Koter, Analysis of an electrodialysis unit on the basis of irreversible thermodynamics, Desalination 95 (1994) 139–153. doi:10.1016/0011-9164(94)00010-7.
URL http://dx.doi.org/10.1016/0011-9164(94)00010-7

[7] H. J. Lee, F. Sarfert, H. Strathmann, S. H. Moon, Designing of an electrodialysis desalination plant, Desalination 142 (2002) 267–286. doi:10.1016/S0011-9164(02)00208-4.
URL http://dx.doi.org/10.1016/S0011-9164(02)00208-4

[8] P. Tsiakis, L. G. Papageorgiou, Optimal design of an electrodialysis brackish water desalination plant, Desalination 173 (2005) 173–186. doi:10.1016/j.desal.2004.08.031.
URL http://dx.doi.org/10.1016/j.desal.2004.08.031

[9] M. Fidaleo, M. Moresi, Optimal strategy to model the electrodialytic recovery of a strong electrolyte, Journal of Membrane Science 260 (2005) 90–111. doi:10.1016/j.memsci.2005.01.048.
URL http://dx.doi.org/10.1016/j.memsci.2005.01.048

[10] R. K. McGovern, A. M. Weiner, L. Sun, C. G. Chambers, S. M. Zubair, J. H. Lienhard V, On the cost of electrodialysis for the desalination of high salinity feeds, Applied Energy 136 (2014) 649–661. doi:10.1016/j.apenergy.2014.09.050.
URL http://dx.doi.org/10.1016/j.apenergy.2014.09.050

[11] J. M. Ortiz, J. A. Sotoca, E. Expósito, F. Gallud, V. García-García, V. Montiel, A. Aldaz, Brackish water desalination by electrodialysis: Batch recirculation operation modeling, Journal of Membrane Science 252 (2005) 65–75. doi:10.1016/j.memsci.2004.11.021.
URL http://dx.doi.org/10.1016/j.memsci.2004.11.021

[12] M. Tedesco, H. Hamelers, P. Biesheuvel, Nernst-Planck transport theory for (reverse) electrodialysis: I. Effect of co-ion transport through the membranes, Journal of Membrane Science 510 (2016) 370 – 381. doi:http://dx.doi.org/10.1016/j.memsci.2016.03.012.
URL http://www.sciencedirect.com/science/article/pii/S0376738816301405

[13] M. Tedesco, H. Hamelers, P. Biesheuvel, Nernst-Planck transport theory for (reverse) electrodialysis: II. Effect of water transport through ion-exchange membranes.
URL arXiv:1610.02833

[14] G. Kraaijeveld, V. Sumberova, S. Kuindersma, H. Wesselingh, Modelling electrodialysis using the Maxwell-Stefan description, The Chemical Engineering Journal and the Biochemical Engineering Journal 57 (1995) 163–176. doi:10.1016/0923-0467(94)02940-7.
URL http://dx.doi.org/10.1016/0923-0467(94)02940-7

[15] P. N. Pintauro, D. N. Bennion, Mass transport of electrolytes in membranes. 2. Determination of sodium chloride equilibrium and transport parameters for Nafion, Industrial & Engineering Chemistry Fundamentals 23 (1984) 234–243. doi:10.1021/i100014a017.
URL http://dx.doi.org/10.1021/i100014a017

[16] R. Krishna, J. Wesselingh, The Maxwell-Stefan approach to mass transfer, Chemical Engineering Science 52 (1997) 861–911. doi:10.1016/S0009-2509(96)00458-7.
URL http://dx.doi.org/10.1016/S0009-2509(96)00458-7

[17] J. Newman, K. E. Thomas-Alyea, Electrochemical systems, John Wiley & Sons, 2012.

[18] E. E. Graham, Use of the Stefan-Maxwell relations to describe ionic transport in ion exchange resins, Ph.D. thesis, Northwestern University (1970).

[19] P. N. Pintauro, D. N. Bennion, Mass transport of electrolytes in membranes. 1. Development of mathematical transport model, Industrial & Engineering Chemistry Fundamentals 23 (1984) 230–234. doi:10.1021/i100014a016.
URL http://dx.doi.org/10.1021/i100014a016

[20] E. E. Graham, J. S. Dranoff, Application of the Stefan-Maxwell equations to diffusion in ion exchangers. 1. Theory, Industrial & Engineering Chemistry Fundamentals 21 (1982) 360–365. doi:10.1021/i100008a007.
URL http://dx.doi.org/10.1021/i100008a007

[21] A. A. Sonin, M. S. Isaacson, Optimization of flow design in forced flow electrochemical systems, with special application to electrodialysis, Industrial & Engineering Chemistry Process Design and Development 13 (1974) 241–248. doi:10.1021/i260051a009.
URL http://dx.doi.org/10.1021/i260051a009

[22] M. S. Isaacson, A. A. Sonin, Sherwood number and friction factor correlations for electrodialysis systems, with application to process optimization, Industrial & Engineering Chemistry Process Design and Development 15 (1976) 313–321. doi:10.1021/i260058a017.
URL http://dx.doi.org/10.1021/i260058a017

[23] O. Kuroda, S. Takahashi, M. Nomura, Characteristics of flow and mass transfer rate in an electrodialyzer compartment including spacer, Desalination 46 (1983) 225–232. doi:10.1016/0011-9164(83)87159-8.
URL http://dx.doi.org/10.1016/0011-9164(83)87159-8

[24] R. A. Robinson, R. H. Stokes, Electrolyte solutions, Courier Corporation, 2002.

[25] T. Shedlovsky, The electrolytic conductivity of some uni-univalent electrolytes in water at 25 C, Journal of the American Chemical Society 54 (1932) 1411–1428. doi:10.1021/ja01343a020.
URL http://dx.doi.org/10.1021/ja01343a020

[26] J. F. Chambers, J. M. Stokes, R. H. Stokes, Conductances of concentrated aqueous sodium and potassium chloride solutions at 25 C, The Journal of Physical Chemistry 60 (1956) 985–986. doi:10.1021/j150541a040.
URL http://dx.doi.org/10.1021/j150541a040

[27] H. B. Callen, Thermodynamics and an introduction to thermostatistics, John Wiley & Sons, 1985.

[28] A. Bejan, Advanced engineering thermodynamics, John Wiley & Sons, 2006.

[29] A. Bejan, Entropy generation through heat and fluid flow, John Wiley & Sons, 1982.

[30] G. C. Ganzi, Electrodeionization for high purity water production, in: AIChE Symposium Series, Vol. 84, 1988.

[31] J. Wood, J. Gifford, J. Arba, M. Shaw, Production of ultrapure water by continuous electrodeionization, Desalination 250 (2010) 973 – 976. doi:10.1016/j.desal.2009.09.084.
URL http://dx.doi.org/10.1016/j.desal.2009.09.084

[32] S. Paoletti, F. Rispoli, E. Sciubba, Calculation of exergetic losses in compact heat exchanger passages, in: ASME AES, Vol. 10, 1989, pp. 21–29.

[33] T. W. Chapman, Transport properties of concentrated electrolytic solutions, Ph.D. thesis, University of California, Berkeley (1967).

[34] R. Mills, V. M. Lobo, Self-diffusion in electrolyte solutions, Elsevier Science, 1989.

[35] K. G. Nayar, M. H. Sharqawy, L. D. Banchik, J. H. Lienhard V, Thermophysical properties of seawater: A review and new correlations that include pressure dependence, Desalination 390 (2016) 1 – 24. doi:10.1016/j.desal.2016.02.024.
URL http://dx.doi.org/10.1016/j.desal.2016.02.024

[36] K. G. Nayar, G. P. Thiel, M. H. Sharqawy, J. H. Lienhard V, Least work of desalination, chemical potential, and flow exergy of seawater, Manuscript in preparation.

[37] G. P. Thiel, E. W. Tow, L. D. Banchik, H. W. Chung, J. H. Lienhard V, Energy consumption in desalinating produced water from shale oil and gas extraction, Desalination 366 (2015) 94 – 112. doi:10.1016/j.desal.2014.12.038.
URL http://dx.doi.org/10.1016/j.desal.2014.12.038

[38] G. P. Thiel, J. H. Lienhard V, Treating produced water from hydraulic fracturing: Composition effects on scale formation and desalination system selection, Desalination 346 (2014) 54 – 69. doi:10.1016/j.desal.2014.05.001.
URL http://dx.doi.org/10.1016/j.desal.2014.05.001

[39] K. S. Pitzer, J. J. Kim, Thermodynamics of electrolytes. IV. Activity and osmotic coefficients for mixed electrolytes, Journal of the American Chemical Society 96 (1974) 5701–5707. doi:10.1021/ja00825a004.
URL http://dx.doi.org/10.1021/ja00825a004

[40] K. S. Pitzer, A thermodynamic model for aqueous solutions of liquid-like density, Reviews in Mineralogy and Geochemistry 17 (1987) 97–142.

[41] C. E. Harvie, J. H. Weare, The prediction of mineral solubilities in natural waters: the Na-K-Mg-Ca-Cl-SO4-H2O system from zero to high concentration at 25 C, Geochimica et Cosmochimica Acta 44 (1980) 981 – 997. doi:10.1016/0016-7037(80)90287-2.
URL http://dx.doi.org/10.1016/0016-7037(80)90287-2

[42] C. E. Harvie, N. Møller, J. H. Weare, The prediction of mineral solubilities in natural waters: The Na-K-Mg-Ca-H-Cl-SO4-OH-HCO3-CO3-CO2-H2O system to high ionic strengths at 25 C, Geochimica et Cosmochimica Acta 48 (1984) 723–751. doi:10.1016/0016-7037(84)90098-X.
URL http://dx.doi.org/10.1016/0016-7037(84)90098-X

[43] K. S. Pitzer, Thermodynamics of electrolytes. I. Theoretical basis and general equations, The Journal of Physical Chemistry 77 (1973) 268–277. doi:10.1021/j100621a026.
URL http://dx.doi.org/10.1021/j100621a026

[44] K. S. Pitzer, J. C. Peiper, R. Busey, Thermodynamic properties of aqueous sodium chloride solutions, Journal of Physical and Chemical Reference Data 13 (1984) 1–102. doi:10.1063/1.555709.
URL http://dx.doi.org/10.1063/1.555709

[45] G. Kraaijeveld, The Maxwell-Stefan description of mass transfer in ion exchange and electrodialysis, Ph.D. thesis, University of Groningen (1994).

List of Figures